



Investigating the effect of geometrical asymmetry on conductance and TMR ratio in the ZnO rock salt-based MTJ: a DFT study

Masoud Ansarino¹

Received: 28 August 2019 / Accepted: 10 June 2020 / Published online: 9 July 2020
© The Author(s) 2020

Abstract

Effects of geometrical asymmetry on spintronic properties of Fe/ZnO/Fe magnetic tunnel junction based on zinc oxide barrier tunnel with rock-salt crystalline structure is studied. Simulations are performed using density functional theory, and substituted layers of C, Mg, Al, Mo, and Ta are used to make geometrically asymmetric structures. The results indicate that this asymmetry has a substantial influence on the properties of the spin-dependent electronic transport, conductance, and the tunneling magneto-resistance (TMR) ratio of the pristine symmetric structure. Additionally, it is shown that geometrical asymmetry results in a sharp decrease in the TMR ratio in one of these junctions and causes a negative TMR ratio in the other four asymmetric structures. Due to the large conductance of the three pristine, C and Al substituted structures in the PA configuration, these structures can be used to generate the current with pure spin for experimental purposes.

Keywords Spintronics · Transport · Rock-salt ZnO · Magnetic tunnel junction (MTJ) · Tunneling magnetoresistance (TMR) · Nanoelectronics

Introduction

In a magnetic tunnel junction (MTJ) device, two ferromagnetic electrodes are separated by a non-magnetic insulator or semiconductor, known as tunnel barrier, with a thickness of about a few nanometers. Electronic transport in MTJs is carried out through quantum tunneling. The left and right electrode's magnetizations might be parallel or antiparallel, resulting in different resistance of MTJs known as tunneling magneto-resistance (TMR) phenomenon, which is an important characteristics of the spintronic devices. Under zero-bias voltage, the TMR ratio is conventionally defined as

$$\text{TMR} = \frac{G_{\text{PA}} - G_{\text{APA}}}{G_{\text{APA}}} \quad (1)$$

where G_{PA} (G_{APA}) is the conductance of the MTJ in parallel (antiparallel) alignment of magnetizations of the electrodes. The type and thickness of barrier layer and the applied bias voltage are important parameters that can affect TMR ratio.

The thickness dependence of magneto-resistance and TMR in MTJs has been investigated [1–5]. Another factor that influences the amount and the sign of TMR ratio is structural asymmetry in MTJs. Moreover, the TMR ratio is usually positive. However, in 1975, Julliere [6] predicted that this ratio can also be negative. This prediction was confirmed in MTJs that are based on magnesium oxide (MgO) and zinc oxide (ZnO) tunnel barriers. Heiliger et al. [7, 8] reported that in the asymmetric junction, independent of the voltage used, the current in the antiparallel alignment configuration (APAC) of the magnetization of electrodes is higher than that it is in their parallel alignment configuration (PAC), which results in a negative TMR ratio. It has been also reported by Waldron et al. [9, 10] that the zero-bias TMR in MgO-based MTJs is substantially reduced by oxidization of the junction interface. This oxidized junction can be also considered as a structural asymmetry.

Owing to its wide band gap (3.37eV), zinc oxide with wurtzite hexagonal crystalline structure is considered as a promising semiconductor material for electronic, optoelectronic, and spintronic applications [11–16]. Moreover, ZnO can have a rock-salt crystalline structure with a wide band gap (2.45eV), which makes it an attractive material to be considered as the non-magnetic tunnel barrier in spintronic and MTJ devices. Magnetic transport properties of rock-salt

✉ Masoud Ansarino
M_Ansarino@Azad.Ac.Ir

¹ Department of Physics, South Tehran Branch, Islamic Azad University, Tehran, Iran

type ZnO-based MTJs (Fe/ZnO/Fe) have been investigated in some experimental and theoretical studies before [17–19]. They showed that the ZnO barrier exhibit coherent tunneling similar to the conventional MgO barrier. However, they did not study the dependence of the magneto-resistance and TMR ratio on the structural asymmetry (with several different asymmetries) of these MTJs.

In this paper, we study the geometrical asymmetry effects on the conductance and TMR ratio in a MTJ based on ZnO with rock-salt structure. We use Fe/ZnO/Fe junction with four ZnO barrier-layer thicknesses as a pristine structure (PS). The elements Magnesium, Carbon, Aluminum, Molybdenum, and Tantalum are used to make geometrically asymmetric substituted structures (SS). The main reason for choosing these materials is that they are commonly used in the electron transport and spintronic applications, and have been shown to affect the TMR ratio of MTJs. It has been shown that [20] C-doped barrier layer can improve conductance of MTJ device. The reason for choosing Mo and Ta is that recent studies [21] have shown that the use of these elements in MTJs can significantly influence TMR and greatly enhance their thermal stability, which is an important parameter in device manufacturing. Finally, since Mg and Al are traditionally used in the manufacture of MTJs [22], it may be useful to investigate the effect of these elements on the spin-dependent behavior of our desired structure.

Computational details

First-principle calculations based on density functional theory (DFT) method are employed to determine the structural, electronic, and transport properties of these MTJs. For our DFT analysis, we use the software package QuantumATK [23] with the PAW pseudopotentials within the GGA for the PBE exchange–correlation functional [24]. For calculating the spin-dependent electronic transport properties through the devices, QuantumATK uses the non-equilibrium Green's

function (NEGF) formalism. The k-mesh for energy integration within the irreducible region of the Brillouin zone (BZ) is chosen as $7 \times 7 \times 2$ for structural optimization and $7 \times 7 \times 100$ for transport calculations. The energy cutoff for separating the core electrons from the valence electrons is set equal to 200 Hartree. Structural optimizations are carried out until atomic force reached below $0.02 \text{ eV}/\text{\AA}$. Self-consistency is achieved when the change in the total energy between cycles of the SCF procedure is reduced to less than 10^{-6} eV .

In pristine structure (PS), two semi-infinite Fe electrodes (in their [001] direction) are attached to the rock-salt ZnO (001) barrier with 4 monolayer (4-ML) thickness (Fig. 1). In this direction, for both up and down spin channels, the Δ_1 (s , p_z , d_{z^2}) symmetry band of Fe plays the dominant role in the electron transport through the barrier [25]. The resulting two-probe device is laterally periodic such that the electrodes are fully three-dimensional in a half plane. Along the Z axis (transmission direction), the two electrodes are semi-infinite. The transverse lattice constants of the device are set equal to the experimental constant of bulk Fe, which is 2.866 \AA .

Structural force optimization calculations are carried out to obtain the optimized central region length, L , as shown in Fig. 1. Three layers of the electrodes at either side of the junction are taken as part of the central region. This is done to eliminate the effects of the barrier region on the electronic structure of the electrodes, enabling a semi-infinite behavior. In the direction parallel to the junction's interface (X – Y plane), periodic boundary conditions are imposed.

To make five asymmetric SSs, the first Zn atom from one side of the barrier is replaced with one of the five C, Mg, Al, Mo and Ta atoms, separately. The unit cell of these MTJs is shown in Fig. 1, where the symbol \boxed{X} stands for atomic elements Zn in PS and one of those five elements in SSs.

The following calculations are performed in our analysis:

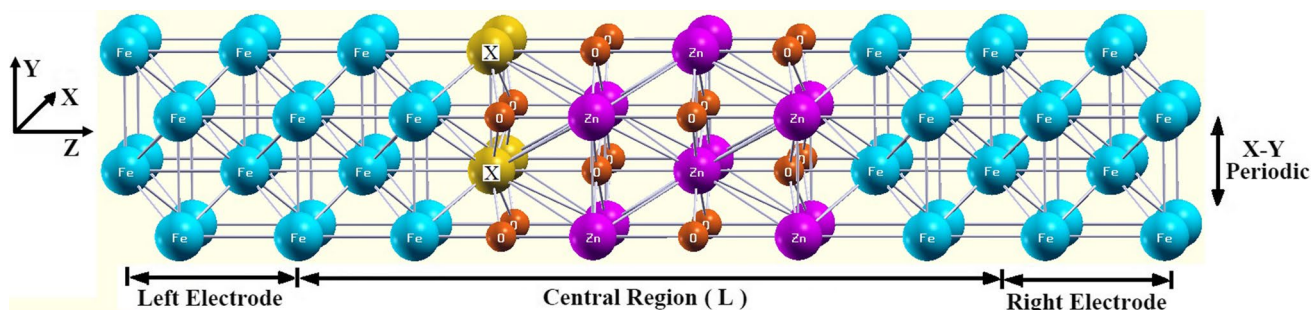


Fig. 1 (Colored) Atomic structure of MTJs with a 4-ML barrier sandwiched between two Fe electrodes. The symbol \boxed{X} stands for atomic elements Zn in PS and C, Mg, Al, Mo and Ta in SSs. The picture

shows the unit cell of MTJ after four repetitions. Two semi-infinite ferromagnetic electrodes are contacted via a central region. 'L' is the length of central region of the device

- (i) Structural force optimization to obtain the optimized central region lengths L ;
- (ii) Mulliken population per spin channel for each atom;
- (iii) Density of states (DOS) of structures for both PA and APA configurations;
- (iv) Energy and k-point-dependent transmission spectrum for both PA and APACs;
- (v) Conductance and TMR ratio of the structures;

To make a PA (APA) configuration, the initial spin of the Fe atoms in both electrodes is considered parallel (antiparallel), and the spin of the other atoms in the device is considered zero.

Results and discussions

The structural optimization of the central region is carried out by fixing the transverse (X – Y plane) lattice constants of the device at the experimental lattice constant of bulk Fe, and allowing the length “ L ” to vary. The above-mentioned optimization process is repeated separately for all six structures and the optimized central region lengths are given in Table 1. In this table and throughout the paper, the structures are arranged by the atomic number of substituted atoms. As can be seen from Table 1, substituted layers cause the L values of all SSs to be greater than that of the PS, with the greatest value belonging to Mg-SS.

To independently adjust the ferromagnetic electrodes’ magnetization in the MTJs in experimental applications, the tunnel barrier must be able to prevent the permeation of magnetization of the electrodes to each other. To this end and to ensure that all atoms in the considered MTJs are correctly spin-polarized in our calculations, Mulliken population per spin channel is calculated for each atom. Mulliken population of atom “ i ” is calculated using the relation $M_i = \sum_{j \in i} \sum_{jm} D_{jm} S_{mj}$, where D and S are the density and overlap matrices, respectively. The sum is taken over all orbitals in the considered atom. The results of this calculation for atoms in the central region of the PS and C-SS in APA and PACs are summarized in Tables 2 and 3, respectively. The difference between spin-up and spin-down populations determines the polarization of each atom, and multiplying this polarization by Bohr magneton gives the magnetic momentum of that atom. From these tables, it can be verified that while Fe atoms are correctly spin-polarized and the atoms next to the interface (on both left and right sides) are slightly affected by magnetization of Fe atoms, the remnant atoms in the barrier far from the interface are un-polarized. Therefore, it can be said that the barrier region is well prevented from penetrating the magnetizations of the two electrodes. Another important point is that the Fe atoms in the left and right electrodes in the PS have completely symmetric spin polarizations, but this symmetry is not present in the SSs. This can affect the spin-dependent transport in these

Table 1 Calculated values of the optimized central region lengths

| | PS | C-SS | Mg-SS | Al-SS | Mo-SS | Ta-SS |
|---------|-------|-------|-------|-------|-------|-------|
| L (Å) | 13.71 | 14.00 | 14.53 | 14.29 | 14.23 | 14.25 |

Table 2 Mulliken atomic populations of the atoms in the central region in the PS. The first and second rows show the spin populations of APA, and the third and fourth rows PACs. All numbers are rounded

| | Fe | Fe | Fe | Zn | O | O | Zn | Zn | O | O | Zn | Fe | Fe | Fe |
|-----------|------|------|------|------|------|------|------|------|------|------|------|------|------|------|
| Spin-up | 5.13 | 5.20 | 5.45 | 5.59 | 3.39 | 3.38 | 5.61 | 5.60 | 3.38 | 3.32 | 5.66 | 2.60 | 2.82 | 2.88 |
| Spin-down | 2.88 | 2.82 | 2.60 | 5.66 | 3.32 | 3.38 | 5.60 | 5.61 | 3.38 | 3.39 | 5.59 | 5.45 | 5.20 | 5.13 |
| Spin-up | 5.13 | 5.20 | 5.45 | 5.59 | 3.39 | 3.38 | 5.61 | 5.61 | 3.38 | 3.39 | 5.59 | 5.45 | 5.20 | 5.13 |
| Spin-down | 2.88 | 2.82 | 2.60 | 5.65 | 3.33 | 3.38 | 5.60 | 5.60 | 3.38 | 3.33 | 5.65 | 2.60 | 2.82 | 2.88 |

Table 3 Mulliken atomic populations of the atoms in the central region in the C-SS. The first and second rows show the spin populations of APA, and the third and fourth rows PACs. All numbers are rounded

| | Fe | Fe | Fe | O | C | O | Zn | O | Zn | O | Zn | Fe | Fe | Fe |
|-----------|------|------|------|------|------|------|------|------|------|------|------|------|------|------|
| Spin-up | 5.03 | 5.22 | 5.32 | 3.04 | 2.04 | 3.20 | 5.66 | 3.34 | 5.66 | 3.30 | 5.76 | 2.65 | 2.84 | 2.87 |
| Spin-down | 2.96 | 2.83 | 2.50 | 3.00 | 2.12 | 3.20 | 5.65 | 3.34 | 5.66 | 3.35 | 5.69 | 5.45 | 5.17 | 5.13 |
| Spin-up | 5.03 | 5.22 | 5.32 | 3.04 | 2.04 | 3.20 | 5.66 | 3.35 | 5.66 | 3.35 | 5.69 | 5.45 | 5.17 | 5.13 |
| Spin-down | 2.96 | 2.83 | 2.50 | 3.00 | 2.12 | 3.20 | 5.65 | 3.34 | 5.66 | 3.30 | 5.76 | 2.65 | 2.84 | 2.87 |

asymmetric devices. The behavior of Mulliken population in the other four SSs is similar to the result shown in Table 3.

To explain the magneto-resistive behavior of the junctions and the effect of geometrical asymmetry, we have calculated the spin-resolved electronic DOS of junctions for PA and APACs. The results for the barrier region are plotted in Figs. 2 and 3, respectively. In all figures, zero of the energy

is shifted to the Fermi level. DOS of up (black curves) and down (red curves) spins in APA configuration of PS in Fig. 2 are completely symmetric, which is one of the spintronics properties of MTJs. But for asymmetric SSs, this behavior is completely eliminated. At the Fermi level of APA configuration, the DOS of all SSs, except Mg-SS, increased compared to that of PS. For the cases of Mo-SS and Ta-SS, the

Fig. 2 (Colored) APAC spin-resolved DOS of barrier region of structures

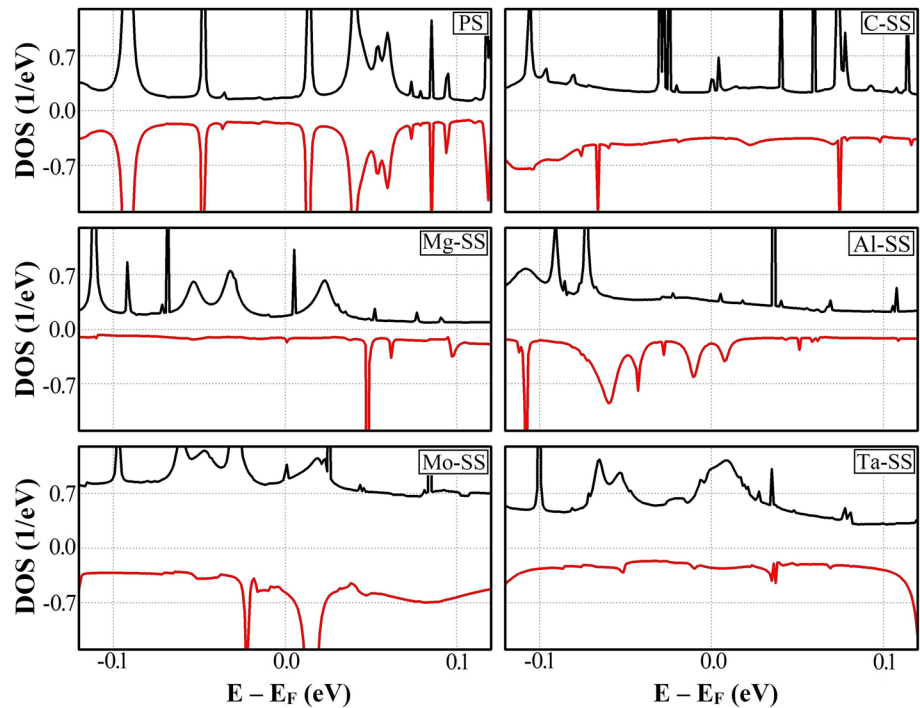
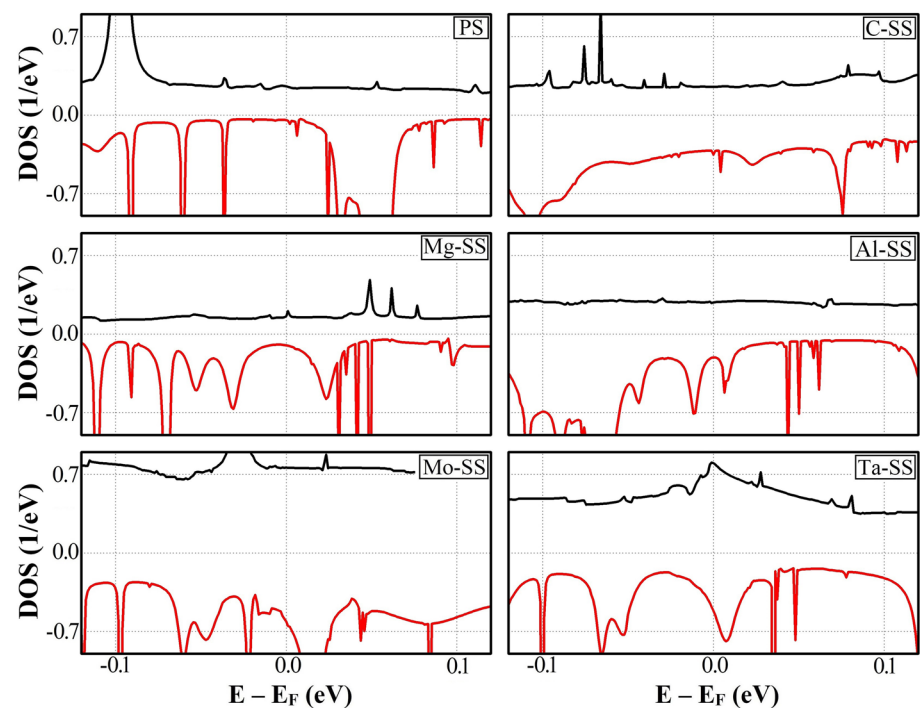


Fig. 3 (Colored) PAC spin-resolved DOS of barrier region of structures



increases are significantly greater than those for other SSs. A similar behavior in increase in DOS is observed at the Fermi level of SSs compared with PS for PA configuration (Fig. 3), except for Mg-SS. For a closer look at the DOS at the Fermi level of PA configuration, these values for all structures are given in Table 4. However, it is important to note that this increase is smaller compared to their APA configuration, and thus can lead to a smaller conductance increase in the PAC of these MTJs compared to their APA configuration.

Next, we study the spin-dependent transport properties of these MTJs by calculating the spin-dependent transmission spectrum of the electrons through the barrier tunnel region as a function of the energy of the electrons. Using Landauer formalism, the spin-dependent transmission probability through the barrier as a function of total energy of the electrons is extracted using the NEGF formalism [26]:

$$T(E) = \text{Tr}[\Gamma_L G^r \Gamma_R G^a] \tag{2}$$

where $G^r(G^a)$ is the retarded (advanced) Green’s function and $\Gamma_L(\Gamma_R)$ is the self-energy of coupling function to the

left (right) electrode. Figures 4 and 5 show the spin-resolved transmission spectrum of these six structures for PA and APACs. As can be seen in Fig. 4, the geometrical symmetry in APAC, caused by the existing symmetry between up and down spin channel’s transmission spectrum in the PS, has been eliminated in the SSs spectrum. Moreover, for both APA and PACs, the SS’s transmission spectrum in the energies smaller than the Fermi level are reduced compared to PS, and increased for the energies greater than the Fermi level. As an important result, a comparison between Figs. 4 and 5 shows that in the Fermi level for all SSs, except C-SS, the transmission in PAC is reduced relative to PS, and significantly increased in APAC. This point affects the change in conductance of the two configurations in SSs relative to the change in PS. For C-SS, although the transmission of PAC in the Fermi level has increased relative to PS, the increase in APAC is much greater than it is in other SSs, for this configuration.

The conductance of a device is calculated using the relation [27]:

Table 4 Calculated values of the DOS at the Fermi level of PA configuration for all structures. The first and second rows show spin-up and spin-down DOS, and the third sum of these values. All numbers are rounded

| | PS | C-SS | Mg-SS | Al-SS | Mo-SS | Ta-SS |
|-----------|-------|-------|-------|-------|-------|-------|
| Spin-up | 0.256 | 0.251 | 0.158 | 0.281 | 0.761 | 0.802 |
| Spin-down | 0.046 | 0.354 | 0.102 | 0.210 | 0.613 | 0.518 |
| sum | 0.302 | 0.605 | 0.260 | 0.491 | 1.374 | 1.320 |

Fig. 4 (Colored) Spin-resolved energy dependent transmission spectrum for APA configuration MTJs with pristine and substituted structures. Black and red curves for up and down spins, respectively

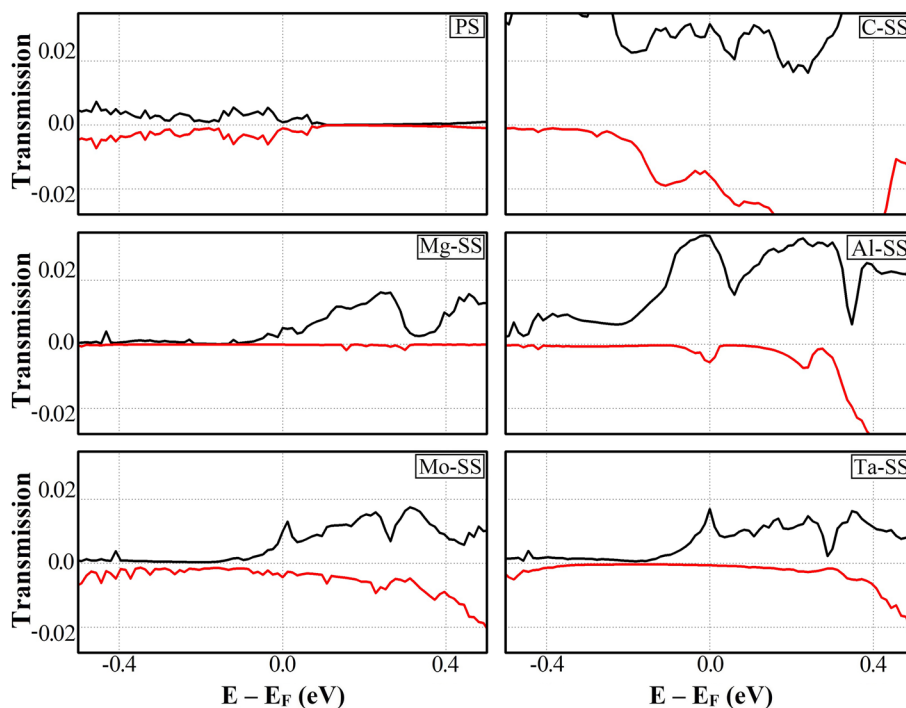
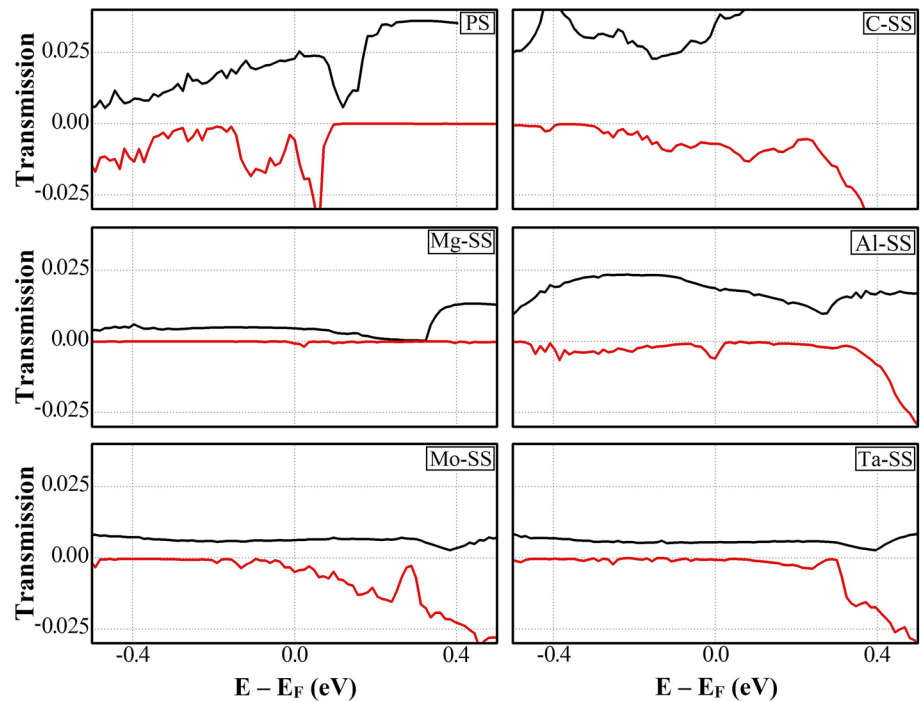


Fig. 5 (Colored) Spin-resolved energy-dependent transmission spectrum for PA configuration MTJs with pristine and substituted structures. Black and red curves for up and down spins, respectively



$$G = \frac{e^2}{h} \sum_{k_{\parallel}} [T(k_{\parallel})]_{E_F} \quad (3)$$

where e and h are electron's charge and Planck's constant, respectively, and $[T(k_{\parallel})]_{E_F}$ is the k_{\parallel} -dependent transmission at the Fermi energy. The k_{\parallel} represents the wave vector components in the first two-dimensional BZ, perpendicular to the transport direction (X – Y plane).

To calculate the MTJ's conductance from Eq. 3, it is necessary to study the transmission spectrum at the Fermi level as a function of the both k_x and k_y . The results of these calculations for the sum of up and down spin transmissions in the APA and PA configurations are plotted in Figs. 6 and 7, respectively. The following results can be extracted from these figures: (1) in the APAC, the geometrical asymmetry causes the transmission peaks of the SSs to be closer to the Γ point and concentrated around it, in comparison with the PS. However, in PAC, these peaks are far from the Γ point and more dispersed; (2) in APA configuration, asymmetry has increased the height of the peaks sharply compared with the PS, and the increase is higher for C-SS and Al-SS than it is for other SSs. Meanwhile, in PAC, the height of the peaks for SSs has decreased compared with PS, and the highest reduction is observed for Ta-SS; (3) for PAC of SSs, except Ta-SS, the transmission peaks are broader than those for PS. In other words, relative to PS, the transmission spectrum of the SSs show larger values in a wider region of BZ, especially for Al-SS; although the peaks have smaller width and are sharper in APA configuration. Given that the

conductivity is calculated by summing the $T(k_{\parallel})$, the above results have important effect on the conductance of both configurations of MTJs.

Figure 8 shows the conductance of all structures calculated using the relation in Eq. 3 for both APA and PACs, and confirm the predictions based on $T(E)$ and $T(k_{\parallel})$ calculations. It can be seen that in PAC, conductance of SSs is reduced relative to PS, except for C-SS. This reduction is more significant for Mg-SS than other structures. For APAC, except Mg-SS, the conductance of all SSs is increased, compared to the conductance of PS. The conductance increase in these configuration is more than it is for related PAC, leading to the negative TMR ratio for these four SSs.

The fact that substituting an Al or C layer in the ZnO-based MTJ can greatly increase its conductance in PAC, or that substituting an Mg layer does not affect the conductance of its APAC severely, but can greatly reduce the PAC conductance which is very useful for experimental applications that require the spin-polarized current.

Using the calculated values for G_{APA} and G_{PA} with the aid of the Eq. 1, the TMR ratio are calculated for all six structures and the results are summarized in Table 5. Two important results are: (1) geometrical asymmetry in these MTJs does not necessarily lead to a negative TMR ratio; and (2) in C-SS structure for which the conductance of both its configurations are greatly increased, the negative TMR ratio is much smaller than that of Ta-SS, with relatively smaller conductance. Therefore, the Ta layer has a better

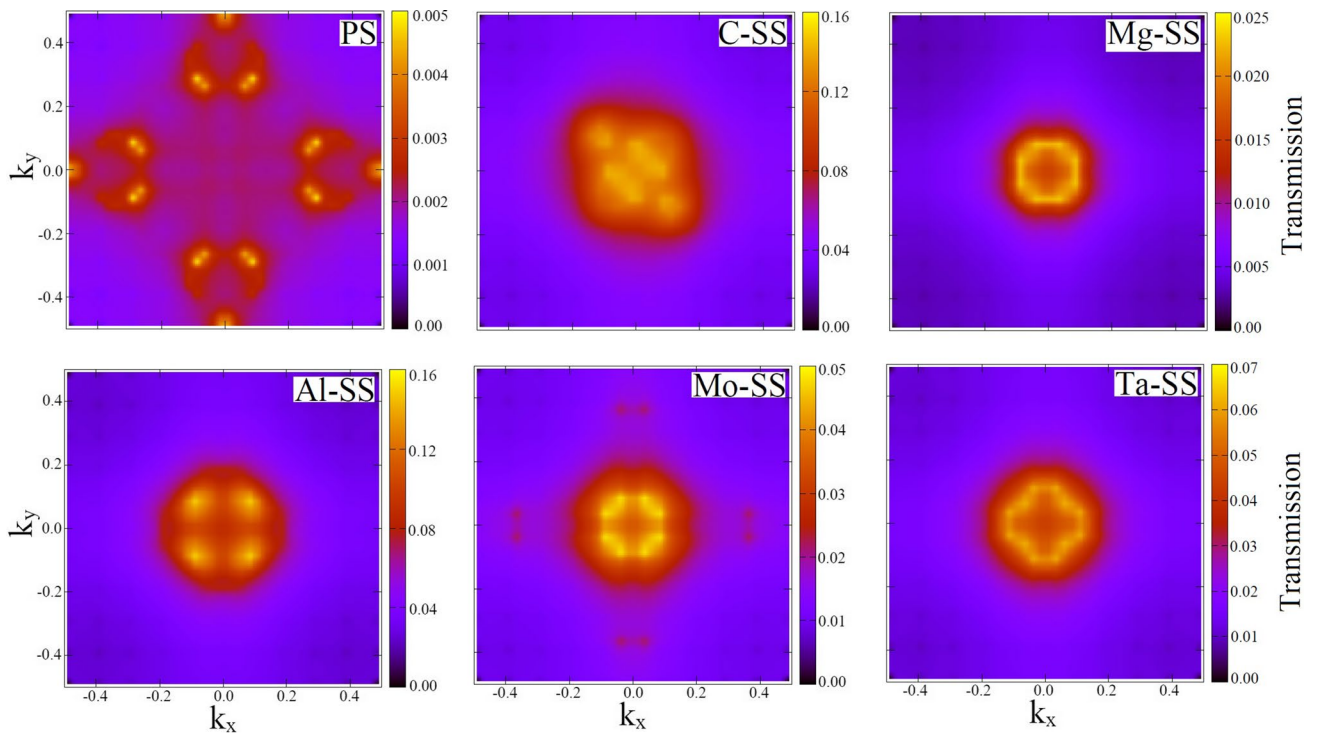


Fig. 6 (Colored) APA configuration k -resolved transmission spectrum of the MTJs within two-dimensional BZ, perpendicular to the transport direction, for sum of up and down spin channels

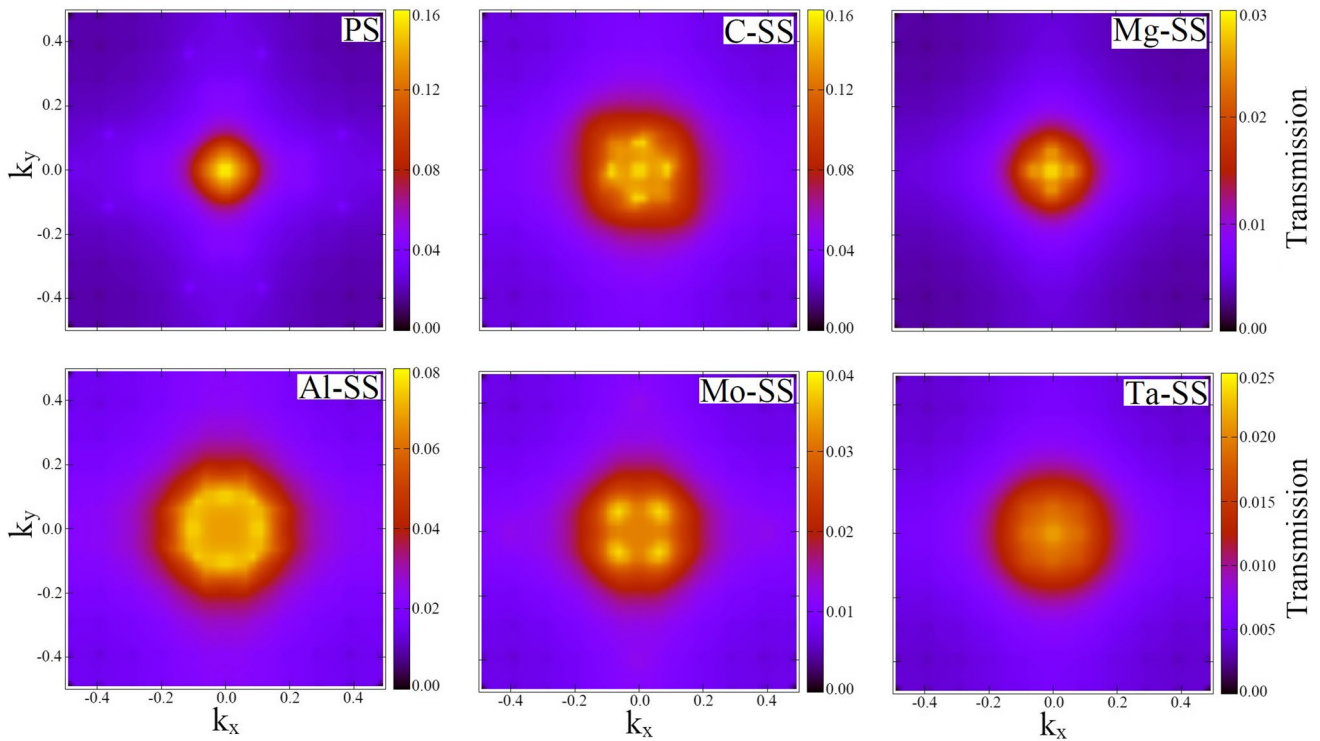


Fig. 7 (Colored) PA configuration k -resolved transmission spectrum of the MTJs within two-dimensional BZ, perpendicular to the transport direction, for sum of up and down spin channels

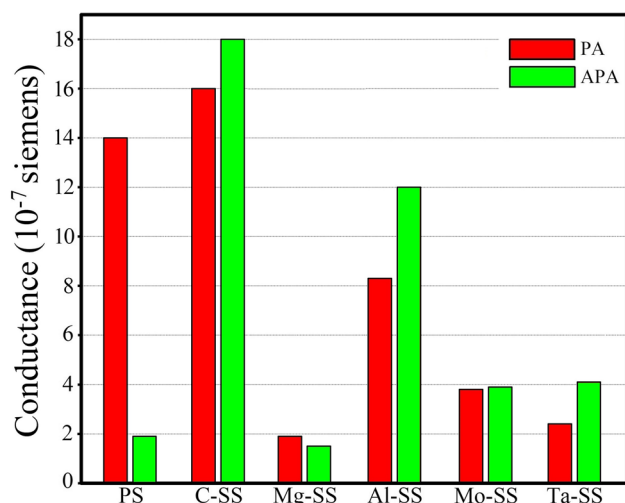


Fig. 8 (Colored) Conductance of PA and APAs for pristine and substituted structures

Table 5 Calculated values of the TMR ratio in percent for pristine and substituted structures

| | PS | C-SS | Mg-SS | Al-SS | Mo-SS | Ta-SS |
|-----------|--------|-------|-------|-------|-------|-------|
| TMR ratio | +636.8 | -11.1 | +26.7 | -30.9 | -2.6 | -41.5 |

functionality than the other three elements for achieving a high negative TMR ratio.

Conclusion

Based on the DFT and NEGF methods, spin-dependent electron transport, conductance, and TMR ratio of one geometrically symmetric and five asymmetric ZnO rock salt-based MTJs are studied. It is shown that substituting the layers of C, Mg, Al, Mo, and Ta in the geometrically symmetric pristine Fe/ZnO(4-ML)/Fe junction, greatly affects transport properties, conductance, and TMR ratio of this device. It is observed that in the asymmetric structures, except for one, conductance in the APAC increases significantly compared to the pristine structure. It is also shown that substituting the Mg layer in PS severely reduces TMR ratio without changing its sign. But in the four other elements, asymmetry changes the sign of the TMR ratio to negative. Due to the large conductance of the PS, C-SS, and Al-SS in the PAC, these structures can be used to generate electric current with pure spin for experimental purposes.

Acknowledgement The author would like to acknowledge Khadijeh Khalili, Technical University of Denmark, for valuable and constructive discussion and comments during calculations and preparation of

this manuscript, and associate Prof Dr. Ahmadi from Computational Nanoelectronic (CoNE) research lab of Universiti Teknologi Malaysia.

Author contributions The author was alone in preparing all the conceptual and computational materials of this study. MA was responsible for performing all the calculations and extracting the results. He was also responsible for writing all parts of the article.

Funding This research did not receive any specific grant from funding agencies in the public, commercial, or not-for-profit sectors.

Open Access This article is licensed under a Creative Commons Attribution 4.0 International License, which permits use, sharing, adaptation, distribution and reproduction in any medium or format, as long as you give appropriate credit to the original author(s) and the source, provide a link to the Creative Commons licence, and indicate if changes were made. The images or other third party material in this article are included in the article's Creative Commons licence, unless indicated otherwise in a credit line to the material. If material is not included in the article's Creative Commons licence and your intended use is not permitted by statutory regulation or exceeds the permitted use, you will need to obtain permission directly from the copyright holder. To view a copy of this licence, visit <http://creativecommons.org/licenses/by/4.0/>.

References

- Butler, W.H., Zhang, X.G., Schulthess, T.C.: Spin-dependent tunneling conductance of Fe/MgO/Fe sandwiches. *Phys. Rev. B* **63**, 054416 (2001)
- Mathon, J., Umerski, A.: Theory of tunneling magnetoresistance of an epitaxial Fe/MgO/Fe(001) junction. *Phys. Rev. B* **63**, 220403 (2001)
- Parkin, S.P., Kaiser, C., Panchula, A.: Giant tunneling magnetoresistance at room temperature with MgO(100) tunnel barriers. *Nat. Mater.* **3**, 862 (2004)
- Ikeda, S., Hayakawa, J., Ashizawa, Y.: Tunnel magnetoresistance of 604% at 300 k suppression of Ta diffusion in CoFeB/MgO/CoFeB pseudo-spin-valves annealed at high temperature. *Appl. Phys. Lett.* **93**, 082508 (2008)
- Wang, T.X., Li, Y., Lee, K.J.: Influence of interface state in Fe/MoO/Fe magnetic tunnel junction system: C modified interface—a first principle study. *J. Appl. Phys.* **109**, 083714 (2011)
- Julliere, M.: Tunneling between ferromagnetic films. *Phys. Lett.* **54A**, 225 (1975)
- Heiliger, C., Zahn, P., Yu, B.: Influence of the interface structure on the bias dependence of tunneling magnetoresistance. *Phys. Rev. B* **72**, 180406 (2005)
- Heiliger, C., Zahn, P., Yu, B.: Interface structure and bias dependence of Fe/MgO/Fe tunnel junctions: Ab initio calculations. *Phys. Rev. B* **73**, 214441 (2006)
- Waldron, D., Timoshevskii, V., Hu, Y.: First principles modeling of tunnel magnetoresistance of Fe/MgO/Fe trilayers. *PRL* **97**, 226802 (2006)
- Waldron, D., Liu, L., Guo, H.: Ab initio simulation of magnetic tunnel junctions. *Nanotechnology* **18**, 424026 (2007)
- Wang, Y., Wang, B., Zhang, Q.: Tunable electronic properties of ZnO nanowires and nanotubes under a transverse electric field. *J. Appl. Phys.* **113**, 034301 (2013)
- Tang, S., Tang, N., Meng, X.: Enhanced power efficiency of ZnO based organic / inorganic solar cells by surface modification. *Phys. E* **83**, 398 (2016)

13. Huang, H., Zhao, Q., Hong, K.: Optical and electrical properties of N-doped ZnO heterojunction photodiode. *Phys. E* **57**, 113 (2014)
14. Sohn, J.I., Choi, S.S., Morris, S.M.: Novel nonvolatile memory with multibit storage based on a ZnO nanowire transistor. *Nano Lett.* **10**, 4316 (2010)
15. Choi, S.H., Jang, B.H., Park, J.S.: Low voltage operating field effect transistors with composite In₂O₃-ZnO-ZnGa₂O₄ nanofiber network as active channel layer. *ACS Nano* **8**, 2318 (2014)
16. Ozgur, U., Alivov, Y.I., Liu, C.: A comprehensive review of ZnO materials and devices. *J. Appl. Phys.* **98**, 041301 (2005)
17. Uehara, Y., Furuya, A., Sunaga, K., Magn, J.: Magnetic tunnel junctions with low resistance-area product of 0.5. *J. Magn. Soc. Jpn.* **34**, 311 (2010)
18. Ansarino, M., Moghaddam, H.M.: The dependence of TMR on the barrier thickness, bias voltage and asymmetry in Fe/ZnO/Fe MTJs: a DFT study. *Phys. E* **107**, 80 (2019)
19. Ansarino, M.: Density functional theory study on the effect of Cu and Na-substituted layers on spin-dependent transport and TMR in the Fe/ZnO/Fe MTJ. *J. Theor. Appl. Phys.* **13**, 375–382 (2019)
20. Dai, Z., Nurbawono, A., Zhang, A.: C-doped ZnO nanowires: electronic structures, magnetic properties, and a possible spintronic device. *J. Chem. Phys.* **134**, 104706 (2011)
21. Almasi, H., Hickey, D.R., Lllige, T.N.: Enhanced tunneling magnetoresistance and perpendicular magnetic anisotropy in Mo/CoFeB/MgO magnetic tunnel junctions. *Appl. Phys. Lett.* **106**, 182406 (2015)
22. Butler, W.H.: Tunneling magnetoresistance from a symmetry filtering effect. *Sci. Technol. Adv. Mater.* **9**, 014106 (2008)
23. Distributed by QuantumWise Company, Copenhagen, Denmark. <https://www.synopsys.com/silicon/quantumatk.html>. Accessed 20 Mar 2018
24. Perdew, J.P., Burk, K., Ernzerhof, M.: Generalized gradient approximation made simple. *Phys. Rev. Lett.* **77**, 3865 (1996)
25. Yuasa, S., Djayaprawira, D.: Giant tunnel magnetoresistance in magnetic tunnel junctions with a crystalline MgO(0 0 1) barrier. *J. Phys. D Appl. Phys.* **40**, R337 (2007)
26. Datta, S.: *Electronic transport in mesoscopic*. Cambridge University Press, Cambridge (1995)
27. Landauer, R.: Spatial variation of currents and fields due to localized scatterers in metallic conduction. *IBM J. Res. Dev.* **1**, 223 (1957)

Publisher's Note Springer Nature remains neutral with regard to jurisdictional claims in published maps and institutional affiliations.